ChinaRxiv

AI translation · View original & related papers at
chinarxiv.org/items/chinaxiv-201611.00252

Effects of Trace Addition of Sn and Nb on the Thermal Stability and Plasticity of Zr-Cu-Fe-Al Bulk Metallic Glass Postprint

Authors: Yang Bin, Li Xin, Luo Wendong, Li Yuxiang

Date: 2016-11-05T00:00:00+00:00

Abstract

Amorphous alloy rods of Zr61.5Cu21.5-xFe5Al11Sn1Nbx (x=0, 1, 2 at.%) and Zr61.5Cu21.5Fe5Al12 with diameters of 2 and 3 mm were prepared by copper mold casting. The results indicate that Sn and Nb microalloying slightly reduces the glass-forming ability of Zr-Cu-Fe-Al amorphous alloys. The Zr61.5Cu19.5Fe5Al11Sn1Nb2 amorphous alloy exhibits excellent compressive plasticity and demonstrates a "strain hardening" phenomenon. High-resolution transmission electron microscopy reveals that both Zr61.5Cu19.5Fe5Al11Sn1Nb2 and Zr61.5Cu21.5Fe5Al12 alloys are fully amorphous, and the atomic packing within the alloy becomes denser after Sn and Nb microalloying. Positron annihilation spectroscopy analysis results demonstrate that, compared with the Zr61.5Cu21.5Fe5Al12 amorphous alloy, the Zr61.5Cu19.5Fe5Al11Sn1Nb2 amorphous alloy exhibits reduced size but increased total amount of interstitial sites between densely packed atoms and structural free volume. The large amount of homogeneously distributed free volume facilitates the formation, branching, and interaction of shear bands in the Zr61.5Cu19.5Fe5Al11Sn1Nb2 amorphous alloy, ultimately improving the plasticity of the amorphous alloy.

Full Text

Effect of Minor Sn and Nb Additions on the Thermal Stability and Compressive Plasticity of Zr-Cu-Fe-Al Bulk Metallic Glass

YANG Bin1,2), **LI Xin**1), **LUO Wendong**1), **LI Yuxiang**1)

1) State Key Laboratory for Advanced Metals and Materials, University of Science and Technology Beijing, Beijing 100083

2) Collaborative Innovation Center of Universal Iron & Steel Technology, University of Science and Technology Beijing, Beijing 100083

Correspondent: YANG Bin, Professor, Tel: (010)62333351, E-mail: byang@ustb.edu.cn

Supported by: Beijing Municipal Natural Science Foundation (No.2122039), the program for ChangJiang Scholars and Innovative Research Team in University and State Key Laboratory for Advanced Metals and Materials, University of Science and Technology Beijing

Manuscript received: 2014-09-02, **in revised form:** 2014-12-30

Abstract

New Ni-free $Zr_{61.5}Cu_{21.5-x}Fe_5Al_{11}Sn_1Nb_x$ (x=0, 1, 2 at%) and $Zr_{61.5}Cu_{21.5}Fe_5Al_{12}$ bulk metallic glasses (BMGs) rods with diameters of 2~mm and 3~mm were fabricated by copper mold casting. In order to improve the plasticity of the $Zr_{61.5}Cu_{21.5}Fe_5Al_{12}$ BMG, minor Sn and Nb elements with lower thermal neutron cross-sections have been added into the Zr-Cu-Fe-Al alloy. The experimental results showed that the glass-forming abilities of the BMGs with Sn and Nb elements were reduced slightly. Among them with Sn and Nb elements, however, $Zr_{61.5}Cu_{19.5}Fe_5Al_{11}Sn_1Nb_2$ BMG exhibits high compressive strength, high ductility together with extensive "work hardening". HRTEM study verifies the glassy states of both $Zr_{61.5}Cu_{19.5}Fe_5Al_{11}Sn_1Nb_2$ and $Zr_{61.5}Cu_{21.5}Fe_5Al_{12}$ alloys samples. The difference between the microstructures of the BMGs samples with and without Sn and Nb elements is that the atomic arrangement in $Zr_{61.5}Cu_{19.5}Fe_5Al_{11}Sn_1Nb_2$ BMG is more closely than that in $Zr_{61.5}Cu_{21.5}Fe_5Al_{12}$ BMG. Positron annihilation lifetime spectroscopy study showed further that the $Zr_{61.5}Cu_{19.5}Fe_5Al_{11}Sn_1Nb_2$ BMG has more closely atomic arrangement than the $Zr_{61.5}Cu_{21.5}Fe_5Al_{12}$ BMG. The structural free-volume size of the former BMG is smaller than that of the latter BMG. And the total free-volume amount of the former BMG is obviously higher than that of the latter BMG. Uniformly distributed free volume is beneficial to improve the shear band formation, branching, and interactions of the $Zr_{61.5}Cu_{19.5}Fe_5Al_{11}Sn_1Nb_2$ BMG, which increases finally the compressive ductility of the BMG.

KEY WORDS: Minor Sn and Nb additions, Zr-Cu-Fe-Al bulk metallic glass, thermal stability, plasticity

---

Introduction

Developed Zr-based bulk metallic glass systems mainly contain elements such as Zr, Cu, Al, Ni, Ti, Fe, Be, and Co, including Zr-Al-Ni(Fe)-Cu, Zr-(Ti,Nb)-Al-

Ni-Cu, Zr-Cu-Al-Ag, Zr-(Pd,Ni)-Cu-Al-Ag, and Zr-Ti-Ni-Cu-Be, with critical sizes reaching the centimeter level. Among these, Zr-Al-Ni-Cu and Zr-Al-Fe-Cu are two Zr-based bulk metallic glass systems with strong glass-forming ability.

Research has shown that Ni in Zr alloys increases hydrogen absorption, leading to hydrogen embrittlement. Based on existing amorphous alloy composition design theories, this work selected the Zr-Cu-Fe-Al system with high glass-forming ability as the research object. Our previous work demonstrated that the prepared $Zr_{61.5}Cu_{21.5}Fe_5Al_{12}$ (abbreviated as Z1) bulk metallic glass possesses high glass-forming ability and thermal stability but exhibits typical brittle fracture behavior.

Microalloying can effectively improve the plasticity of Zr-based bulk metallic glasses, but there are few public reports on simultaneously adding Sn and Nb as alloying elements to Zr-based amorphous alloys to improve comprehensive properties (plasticity, corrosion resistance, etc.). The main alloying elements in zirconium alloys for nuclear fuel assemblies are Sn (0.65~b) and Nb (1.1~b) with small thermal neutron absorption cross-sections. For example, Zr-2 and Zr-4 alloys contain 1.2%$_{1.5}$wt% Sn, Zr-1Nb alloy contains about 1~wt% Nb, Zr-2.5Nb alloy contains about 2.5~wt% Nb, and new zirconium alloys such as ZIRLO and E635 are Zr-Sn-Nb series alloys with Sn and Nb contents around 1~wt%. Adding small amounts of Sn and Nb to pure Zr can significantly improve mechanical properties and corrosion resistance. This work adopts the microalloying approach of Sn and Nb (substituting for some Al and Cu atoms in the $Zr_{61.5}Cu_{21.5}Fe_5Al_{12}$ amorphous alloy) to design the $Zr_{61.5}Cu_{21.5-x}Fe_5Al_{11}Sn_1Nb_x$ (x=0, 1, 2 at%) series alloys, investigating the thermal stability and plasticity of Zr-Cu-Fe-Al-Sn-Nb bulk metallic glasses.

High-purity metals Zr (99.9%), Cu (99.98%), Fe (99.9%), Al (99.99%), Sn (99.99%), and Nb (99.9%) were placed in a WKDHL-2 high-vacuum arc furnace and melted according to composition ratios. The melting atmosphere was high-purity Ar (99.999%) after titanium oxygen consumption. Each alloy ingot was melted four times to ensure composition uniformity. Rod-shaped alloy samples were prepared by differential pressure suction casting with diameters of 2~mm and 3~mm.

X-ray diffraction confirmed that the obtained rod samples were fully amorphous. The amorphous rods were cut into 1~mm thick discs using a low-speed precision cutting machine, then ground with sandpaper, polished, ultrasonically cleaned, dried, and stored. Phase composition of the 3~mm diameter rods was examined using a D/MAX-RB X-ray diffractometer (XRD). Glass transition temperature T_g and crystallization onset temperature T_x were measured using a NETZSCH STA 449 C/CD differential scanning calorimeter (DSC). Compressive properties were tested using a CMT4305 electronic universal testing machine. Compression specimens were cylindrical samples with 2~mm diameter and 4~mm height at a strain rate of 4×10^{-4}~s^{-1}. Three specimens were tested to ensure reliability. Fracture morphology of compressed specimens was observed using a SUPRA55 field emission scanning electron microscope (SEM). Microstructure and selected

area electron diffraction patterns (SADP) were examined using a JEM 2010 high-resolution transmission electron microscope (HRTEM) at 200~kV accelerating voltage. Free volume inside the amorphous alloys was analyzed using a positron annihilation lifetime spectrometer (developed by the Institute of High Energy Physics, Chinese Academy of Sciences, with EG&G ORTEC NIM modules as the core). Positron annihilation lifetime spectroscopy was performed on a fast-slow coincidence spectrometer with a resolution of 196.6~ps. Each spectrum accumulated 2 million counts for good statistics. Fitting software was the universal LT9.0.

2.1 Effect of Minor Sn and Nb Additions on Thermal Stability of Zr-Cu-Fe-Al Amorphous Alloys

[FIGURE:1] shows the XRD patterns of the $Zr_{61.5}Cu_{21.5-x}Fe_5Al_{11}Sn_1Nb_x$ series alloys and the Z1 amorphous alloy. Only the $Zr_{61.5}Cu_{19.5}Fe_5Al_{11}Sn_1Nb_2$ alloy (abbreviated as Z2) exhibits a fully amorphous structure. The figure shows that adding 1~at% Sn to the Zr-Cu-Fe-Al amorphous alloy results in the appearance of $AlZr_2$, $AlZr_3$, Al_{3Zr}, and $ZrCu$ phases. As Nb content increases, the intensity of crystalline phase peaks weakens. When Nb content increases to 2~at%, the Z2 alloy has a complete amorphous structure.

[FIGURE:2] presents the DSC curves of the Z2 and Z1 amorphous alloys. The results show that minor Sn and Nb additions transform the primary crystallization behavior from one-stage to two-stage. The thermodynamic parameters and thermal neutron absorption cross-section data for the two amorphous alloys are listed in . Compared with the Z1 amorphous alloy, the primary crystallization temperature T_{x1} of the Z2 amorphous alloy decreases by 12~K, the supercooled liquid region ΔT_x decreases by 10~K, and both the reduced glass transition temperature T_{rg} ($T_{rg} = T_g/T_l$, where T_g is the glass transition temperature and T_l is the liquidus temperature) and the γ parameter [$\gamma = T_x/(T_g + T_l)$, where T_x is the crystallization onset temperature] decrease slightly. This indicates that Sn and Nb microalloying slightly reduces the glass-forming ability of Zr-Cu-Fe-Al amorphous alloys, while T_g, melting point T_m, and T_l remain almost unchanged. also shows that the thermal neutron absorption cross-section (σ_a) of the Z2 amorphous alloy is smaller than that of the Z1 amorphous alloy, which is beneficial for developing new Zr-based amorphous alloys for irradiation resistance applications.

shows the DSC curves of the Z2 amorphous alloy at different heating rates. The Kissinger plots constructed from T_g, T_x, first crystallization peak temperature T_{p1}, and second crystallization peak temperature T_{p2} at different heating rates are shown in [FIGURE:4]. The apparent activation energy values at each characteristic temperature for the Z2 amorphous alloy were obtained by calculating the slopes and are listed in , along with the apparent activation energies for the Z1 amorphous alloy. The results indicate that both Z2 and Z1 amorphous

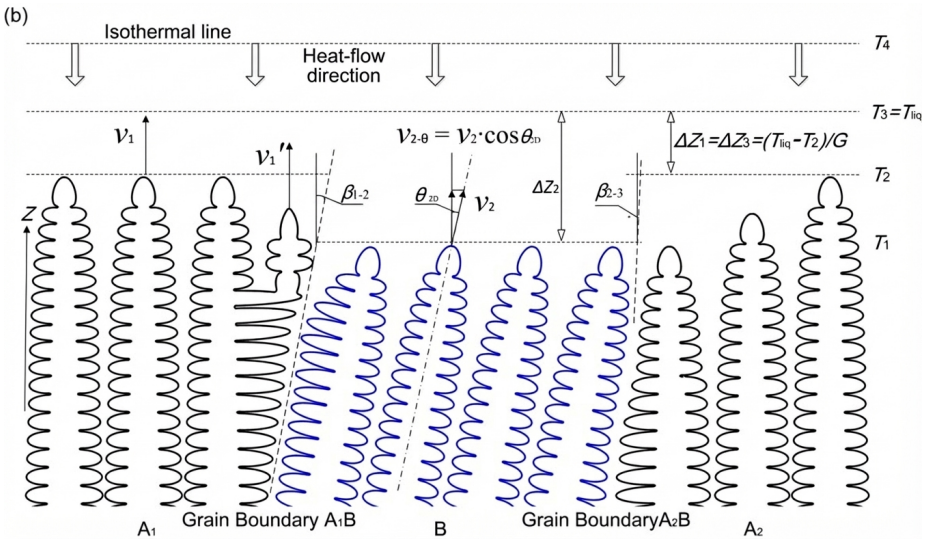

Figure 1: Figure 3

alloys possess good anti-crystallization ability and high thermal stability. The apparent activation energy for glass transition (E_g) and crystallization onset (E_{x1}) of the Z2 amorphous alloy are slightly lower than those of the Z1 amorphous alloy, suggesting that minor Sn and Nb additions slightly decrease the anti-crystallization ability of the amorphous alloy.

2.2 Effect of Minor Sn and Nb Additions on Plasticity of Zr-Cu-Fe-Al Amorphous Alloys

[FIGURE:5] shows the engineering stress-strain curves of the Z2 and Z1 amorphous alloys at a strain rate of 4×10^{-4}~s^{-1}. The Z1 amorphous alloy exhibits brittle fracture behavior, whereas the Z2 amorphous alloy demonstrates excellent compressive plasticity and shows a "strain hardening" phenomenon.

The compressive mechanical properties of the Z2 and Z1 amorphous alloys are listed in . The maximum compressive stress σ_{max} and fracture strain ε_f of the Z2 amorphous alloy are much higher than those of the Z1 amorphous alloy. The elastic modulus E and yield strength σ_y are slightly lower than those of the Z1 amorphous alloy. Notably, the σ_{max} of the Z2 amorphous alloy far exceeds its yield strength σ_y, exhibiting a "strain hardening" phenomenon, which is very rare in bulk metallic glasses.

---

3. Analysis and Discussion

The effective suppression of $AlZr_2$, $CuZr$, and $FeZr_2$ phase precipitation by Nb addition is attributed to the negative mixing enthalpies of $Nb-Al$, $Nb-Fe$, and $Nb-Sn$, which are −16, −18, and −1~kJ/mol, respectively. According to Inoue' s empirical rules for amorphous formation, adding Nb to Zr-Cu-Fe-Al-Sn alloys is beneficial for obtaining amorphous microstructures.

Most previously reported bulk metallic glasses show stress decreasing with shear band softening during plastic deformation, without obvious strain hardening. In 2005, Das et al. first discovered significant "work hardening" in $Cu_{47.5}Zr_{47.5}Al_5$ bulk metallic glass, attributing it to atomic-scale heterogeneity in the amorphous structure that leads to massive shear band formation and strong interactions.

a and c show the HRTEM images and corresponding SAD patterns of the Z2 and Z1 amorphous alloys. The results demonstrate that the alloy maintains a fully amorphous structure after Sn and Nb microalloying.

b and d reveal that compared with the Z1 amorphous alloy, the Z2 amorphous alloy has more closely packed atomic arrangements with more short-range ordered atomic clusters.

[FIGURE:7] shows the fracture morphologies of the compressed Z2 and Z1 amorphous alloys. The Z2 amorphous alloy exhibits shear bands and their intersections, as shown in [FIGURE:7]a. This occurs because adding relatively large Sn and Nb atoms helps hinder the diffusion of smaller Cu and Fe atoms, making the free volume distribution more uniform, increasing shear band nucleation sites, and promoting shear band multiplication. [FIGURE:7]b shows numerous shear bands piled up in region B and extended in region C, similar to dislocation pile-up and intersection phenomena during deformation of crystalline metallic materials. The Z1 amorphous alloy shows highly localized shear fracture behavior with a fracture plane angle of approximately 43° relative to the stress axis, as shown in [FIGURE:7]c. [FIGURE:7]d displays the typical vein pattern fracture morphology of the Z1 amorphous alloy. It is well known that "work hardening" in crystalline metallic materials results from numerous grain boundaries and second-phase particles, where dislocation slip easily piles up, causing dislocation intersections that increase deformation resistance. However, bulk metallic glasses lack grain boundaries, and

shows no second-phase particles after Sn and Nb microalloying. Therefore, this "work hardening" behavior may be related to randomly distributed free volume in the amorphous alloy.

Beukel et al. pointed out that structural relaxation and glass transition phenomena in DSC curves can be explained by the free volume model. The average free volume per atom Δv_f is proportional to the relaxation enthalpy ΔH, i.e., $\Delta H = \beta \cdot \Delta v_f$, where β is a constant for a specific alloy. Slipenyuk et al. confirmed the linear relationship between Δv_f and ΔH by measuring the density of $Zr_{55}Cu_{30}Al_{10}Ni_5$ amorphous alloy at different annealing degrees. Therefore,

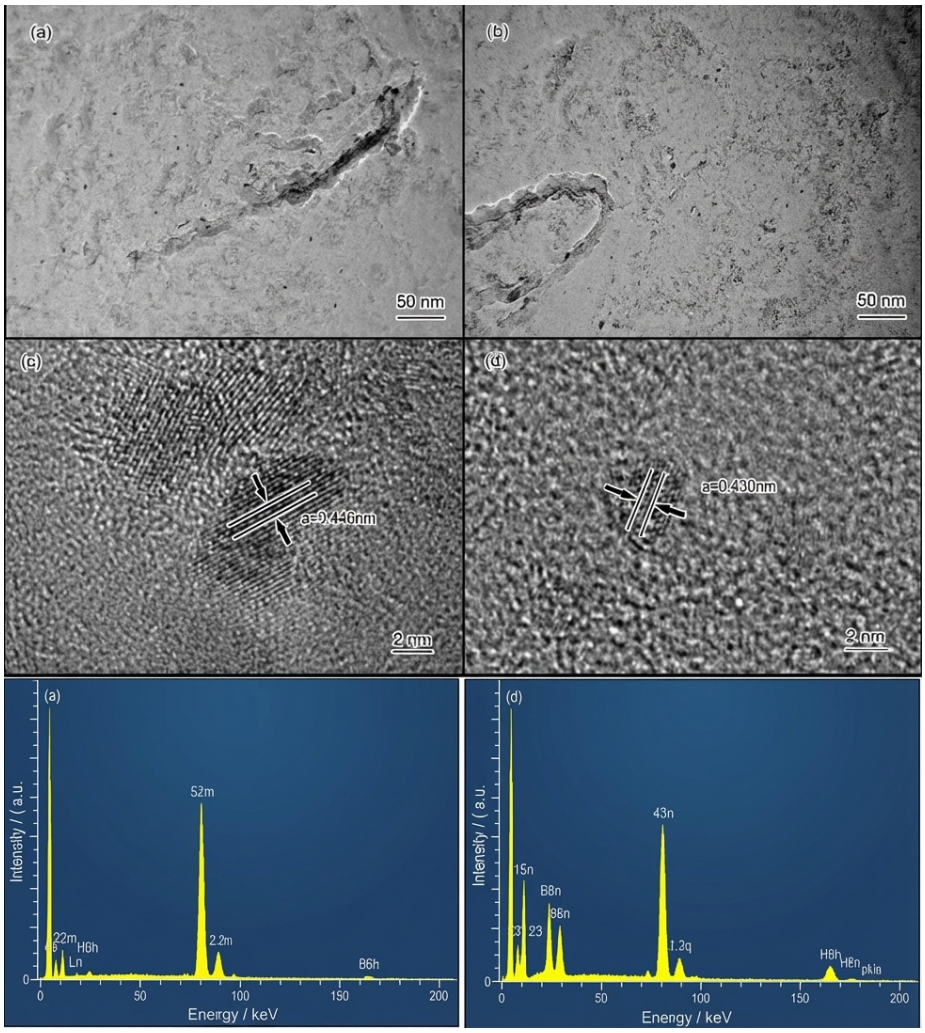

Figure 2: Figure 6

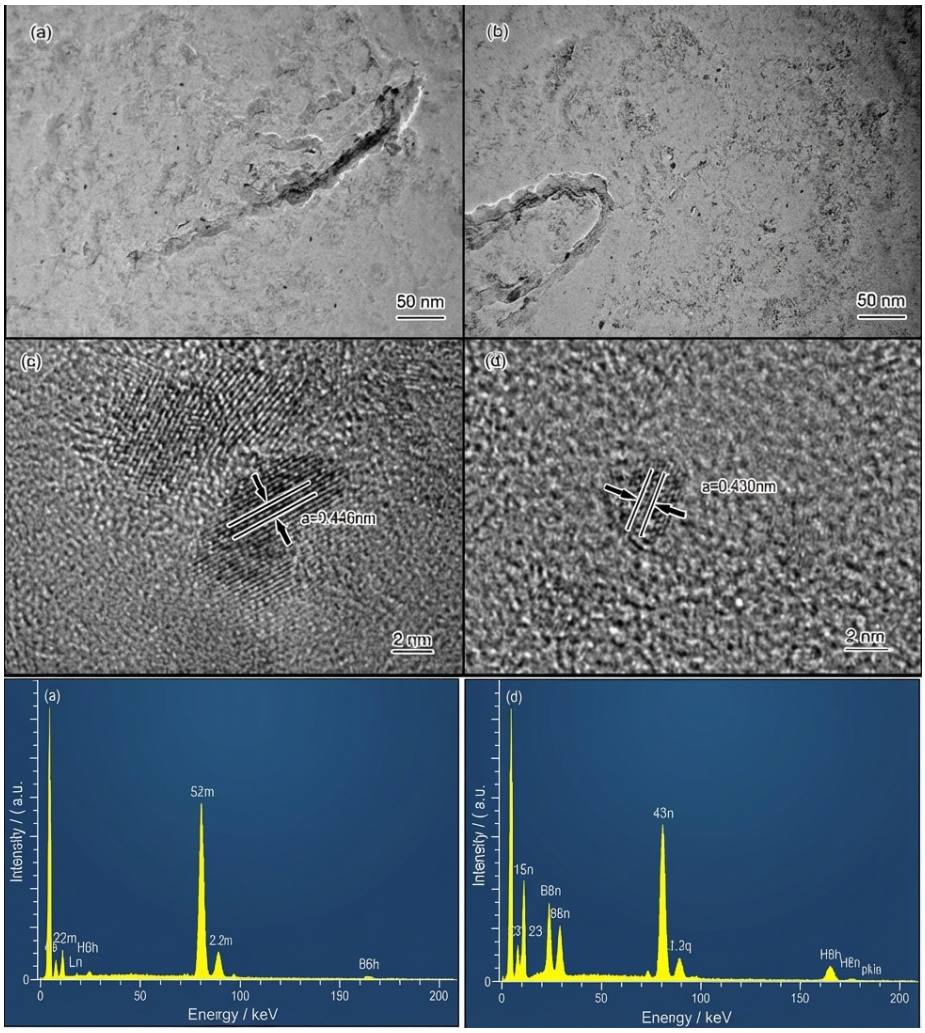

Figure 3: Figure 6

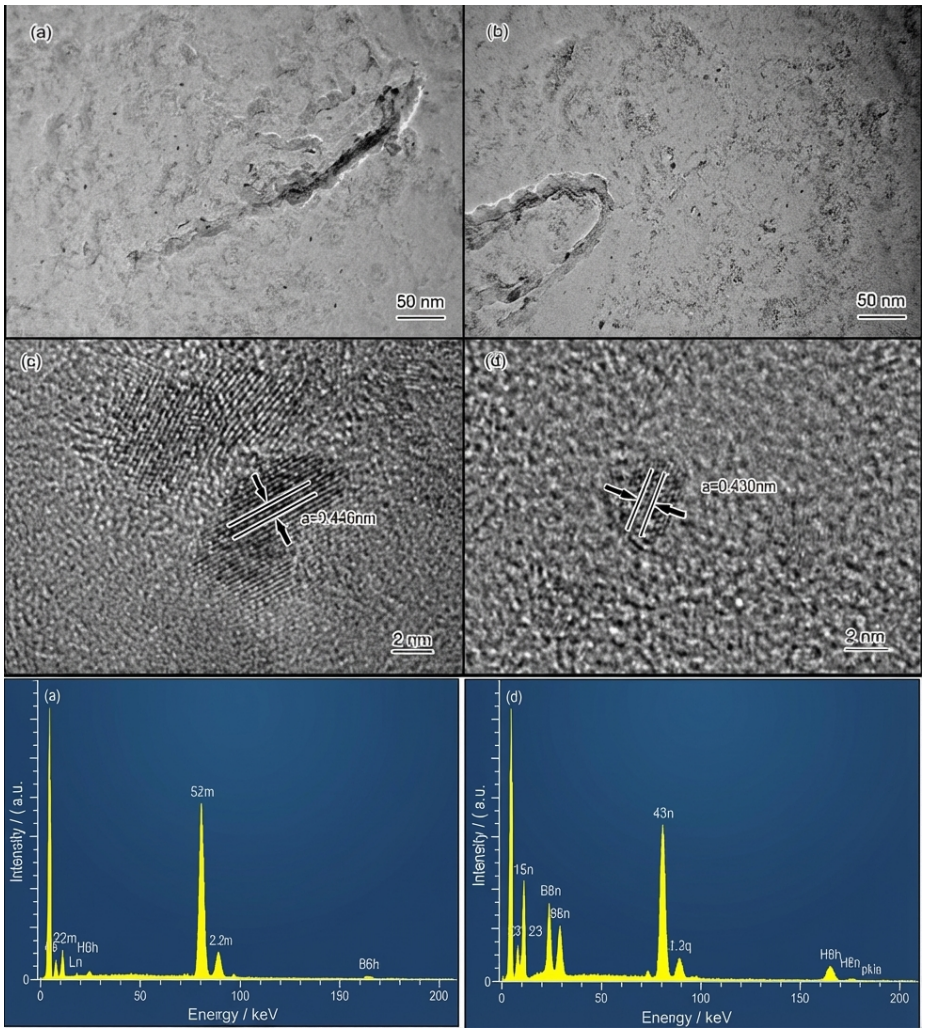

Figure 4: Figure 6

the relative magnitude of structural relaxation energy can be used to characterize the trend of free volume changes.

The DSC curves of the Z2 and Z1 amorphous alloys are shown in [FIGURE:8]. Both curves exhibit exothermic peaks characteristic of structural relaxation. The glass transition temperatures of the two amorphous alloys are similar (see). The inset in [FIGURE:8] shows that the area of the relaxation exothermic peak for the Z2 amorphous alloy is significantly larger than that for the Z1 amorphous alloy, indicating that the Z2 amorphous alloy releases more energy during structural relaxation and thus contains more free volume. However, DSC results only demonstrate increased total free volume in the Z2 amorphous alloy but cannot provide information on vacancy types and their distribution, requiring further analysis by positron annihilation techniques.

Three different types of vacancies exist in amorphous alloys: atomic dense-packed interstices, structural free volume, and nanopores. Structural free volume and atomic dense-packed interstices are the two main types. Structural free volume consists of Bernal voids remaining from random atomic packing or defects caused by structural flow, with relatively large sizes and thus longer positron annihilation lifetimes (τ_i). Atomic dense-packed interstices mainly exist in ordered atomic structures of amorphous alloys with relatively small sizes and thus shorter positron annihilation lifetimes. The magnitude of τ_i reflects the average size of these vacancies, while the intensity I_i corresponding to the i-th lifetime component reflects their concentration.

presents the three-lifetime component fitting results of positron annihilation spectroscopy for the Z2 and Z1 amorphous alloys. τ_3 represents the lifetime of nanopores. Since its proportion (I_3) is small and the difference in τ_3 intensity between the two alloys is negligible, it is ignored in this analysis. τ_2 lifetime is greater than the positron annihilation lifetime at lattice vacancies in pure iron ($V_{Fe} = 165$~ps) and is considered as annihilation lifetime at relatively large structural free volume. τ_1 lifetime is smaller and is considered as annihilation lifetime at relatively small atomic dense-packed interstices.

The results show that after Sn and Nb microalloying, the positron annihilation lifetime of the Z2 amorphous alloy decreases, indicating that both structural free volume and atomic dense-packed interstice sizes are reduced. To further illustrate changes in free volume size and quantity after Sn and Nb microalloying, two-lifetime fitting of the positron annihilation lifetime spectra was performed to obtain the average lifetime value τ_m and intensity of positrons annihilating in free volume (). The magnitude of τ_m reflects changes in overall free volume size, while its intensity reflects changes in overall free volume quantity. shows that after Sn and Nb microalloying, τ_m decreases from 176.4~ps to 168.3~ps, while the intensity of τ_m increases from 98.68% to 98.77%.

Comparing the two sets of lifetime values in for the Z2 and Z1 amorphous alloys reveals that both τ_1 and τ_2 lifetimes of the Z1 amorphous alloy are longer than those of the Z2 amorphous alloy, indicating relatively larger atomic spac-

ing and looser atomic packing in the Z1 amorphous alloy, with larger structural free volume and atomic dense-packed interstice sizes. Comparing the lifetime intensities of the two amorphous alloys shows that after Sn and Nb microalloying, I_1 increases while I_2 decreases, indicating that Sn and Nb microalloying increases the quantity of structural free volume while reducing its size, meaning the structural free volume distribution in the Z2 amorphous alloy becomes more dispersed. Evidently, large amounts of uniformly distributed free volume are beneficial for shear band formation, branching, and interactions, ultimately improving the plasticity of the amorphous alloy.

Conclusions

1. The $Zr_{61.5}Cu_{19.5}Fe_5Al_{11}Sn_1Nb_2$ amorphous alloy has slightly lower anti-crystallization ability compared with the $Zr_{61.5}Cu_{21.5}Fe_5Al_{12}$ amorphous alloy.
2. Compared with the $Zr_{61.5}Cu_{21.5}Fe_5Al_{12}$ amorphous alloy, the $Zr_{61.5}Cu_{19.5}Fe_5Al_{11}Sn_1Nb_2$ amorphous alloy exhibits reduced atomic dense-packed interstice size, decreased structural free volume size, and increased total free volume amount.
3. After minor Sn and Nb additions, large amounts of uniformly distributed free volume facilitate shear band formation, branching, and interactions, ultimately improving the plasticity of Zr-Cu-Fe-Al amorphous alloys.

References

[1] Zhang Q S, Zhang W, Inoue A. Scr. Mater., 2009;61: 241
[2] Inoue A, Zhang Q S, Zhang W, Yubuta K, Son K S, Wang X M. Mater. Trans., 2009;50: 388
[3] Wang W H, Prog. Mater. Sci., 2012;57:487
[4] Jiang Q K, Wang X D, Nie X P, Zhang G Q, Ma H, Fecht H J, Bendnarcik J, Franz H, Liu Y G, Can Q P, Jiang J Z. Acta Mater., 2008;56: 1785
[5] Zhang Q S, Zhang W, Inoue A. Mater. Trans.,2008; 49: 2743
[6] Johnson W L. MRS Bull., 1999;24: 42
[7] Liu J Z. Nuclear Structural Materials. Beijing: Chemical Industry Press, 2007:162 (刘建章. 核结构材料. 北京: 化学工业出版社, 2007: 162)
[8] Chen H M, Ma C L, Bai X D. Corrosion and Protection of Nuclear Reactor Materials. Beijing: Atomic Energy Press, 1984:222 (陈鹤鸣，马春来，白新德. 核反应堆材料腐蚀及其防护. 北京: 原子能出版社, 1984:222)
[9] Luo W D, Yang B, Chen GL, Scr. Mater., 2011;64:625
[10] Luo W D, Master thesis, University of Science and Technology Beijing, Beijing, 2010 (罗文东. 北京科技大学硕士学位论文, 北京, 2010)
[11] Wu X F, Zhang H F, Qiu K Q, Yang H C, Hu Z Q, Acta Metall Sin.,

2003;39:555 (武晓峰, 张海峰, 邱克强, 杨洪才, 胡壮麒, 金属学报, 2003;39:555)
[12] Liu Y H, Wang G, Pan M X, Wang W H, Science, 2007;315:1385
[13] Wang W H, Prog. Sci., 2013;33:177 (汪卫华, 物理学进展, 2013;33:177)
[14] Kondo R, Nomura S N, Tsutsumi Doi Y H, Hanawa T, Acta Biomater., 2011;7:4278
[15] Zhou F Y, Wang B L, Qiu K J, Lin W J, Li L, Wang Y B, Nie F L, Zheng Y F, Mater. Sci. Eng. C, 2012;32:851
[16] Wei J, Frankel P, Polatidis Blat E M, Ambard A, Comstock R J, Hallstadius L, Hudson D, Smith G D W, Grovenor C R M, Klaus M, Cottis R A, Lyon Preuss S M, Acta Mater., 2013;61:4200
[17] Inoue A. Proc. Jpn. Acad. B, 1997;73:19
[18] Inoue A. Bulk Amorphous Alloys: Preparation and Fundamental Characteristics. Uetikon-Zurich: Trans Tech Publications, 1998:3
[19] Suryanarayana C, Inoue A. Bulk Metallic Glass. New York: CRC Press, 2011:67
[20] Chen H, He Y, Shiftlet G J, Poon S J, Nature, 1994; 367: 541
[21] Das J, Tang M B, Kim K B, Theissmann R, Baier F, Wang W H, Eckert J, Phys. Rev. Lett., 2005; 94: 205501
[22] Chen L Y, Fu Z D, Zhang G Q, Hao X P, Jiang Q, Wang X D, Cao Q P, Franz H, Liu Y G, Xie H S, Zhang S L, Wang B Y, Zeng Y W, Jiang J Z, Phys. Rev. Lett., 2008; 100: 075501
[23] Hui X, Liu S N, Pang S J, Zhuo L C, Zhang T, Chen G L, Liu Z K, Scr. Mater., 2010; 63: 239
[24] Beukel A V D, Sietsma J. Acta Metall. Mater., 1990;38:383
[25] Slipenyuk A, Eckert J. Scr. Mater., 2004;50:39
[26] Daniel B S S, Reger-Leonhard A, Heilmaier M, Eckert J, Schultz L. Mech. Time-Depend. Mater., 2002;6:193
[27] Flores K M, Sherer E, Bharathula A, Chen H, Jean Y C. Acta Mater., 2007;55:3403
[28] Li Y X, Master thesis, University of Science and Technology Beijing, Beijing, 2011 (李宇翔. 北京科技大学硕士学位论文, 北京, 2011)

Source: ChinaXiv —Machine translation. Verify with original.